JOURNAL OF MATERIALS SCIENCE 35 (2000) 5945–5950

DC field dependence of dielectric constant and loss factor of Al_2O_3-doped barium strontium titanate for application in phased array antennas

LONG WU, SEAN WU, FENG-CHIH CHANG, YU-TANG SHEN, YIH-CHIEN CHEN
Department of Electrical Engineering, National Cheng-Kung University, Tainan 70101, Taiwan, Republic of China
E-mail: piezo@mail.ncku.edu.tw

DC electric field effects on the real part of the relative dielectric constant and the loss factor of barium strontium titanate for application in phased array antennas have been studied. The real part of the relative dielectric constant of the specimens decreases with increasing applied DC field. The loss factor under bias DC electric field is slighter than the real part of the relative dielectric constant does. The tunability is about 24% for barium strontium titanate doped with 1 wt% Al_2O_3 content. Variation of fitted phenomenological coefficients with Al_2O_3 contents below 10 wt% is small and a rapid increase of the fitted phenomenological coefficient occurs above 10 wt%. Variation of field coefficient A and tunability with Al_2O_3 contents has the same trend as that of the grain size. The real part of the relative dielectric constant of Al_2O_3 doped barium strontium titanate decreases rapidly before 1.0 KV/cm and slowly after 1 KV/cm compare to the data obtained by the curve fitting. There is a conduction loss mechanism other than the intrinsic dielectric loss for the dielectric loss under bias electric field.

1. Introduction

Phased array antennas are currently constructed using ferrite phase-shifting elements. However, these are very costly, large, and heavy. In order to make these devices practical for commercial and military uses; better materials must be developed [1]. The desirable characteristics of a dielectric material for phased array applications would be low dielectric constant, low dielectric loss factor and high dielectric tunability. The tunability of the specimen affects its properties through changes of the dielectric constant with applied electric field. The phase-shifting ability is directly related to the tunability; therefore, higher tunabilities are desirable [2]. Reduction of the dielectric constant reduce the overall impedance mismatch. The loss tangent serves to dissipate or absorb the incident microwave energy; thus a low loss tangent serves to decrease the insertion loss [3]. Numerous studies on the dielectric properties of $(Ba_{1-x}Sr_x)TiO_3$-based ceramics using the conventional mixed oxide method have been carried out. The real part of the relative dielectric constant of $Ba_xSr_{1-x}TiO_3$ ceramics varies from 200 to 900, and the loss factor of $Ba_xSr_{1-x}TiO_3$ ceramics varies from 10^{-3} to 10^{-2} around 2 GHz [4]. The real part of the relative dielectric constant of samples doping with a small amount of phosphor sintered at 1150 and 1200 °C are 6100 and 5500, respectively [5]. Fe_2O_3-doped $(Ba_{0.6}Sr_{0.4})TiO_3$ produced the smallest loss factor of all the dopants studied included Mn, Bi, Ga, Y, Nb and Fe [6]. Al_2O_3-doped $(Ba_{0.6}Sr_{0.4})TiO_3$ materials exhibit behavior which renders them suitable for use in phased array antennas. The improved properties of these samples include a low real part of the relative dielectric constant, a low loss factor and high tunability [7]. Based on the results, further investigations on $(Ba_{0.6}Sr_{0.4})TiO_3$ doped with Al_2O_3 have been made to produce ceramics with better dielectric properties for application in phased array antennas. For perovskite structures (ABO_3), doping with small amounts of acceptor ions on B sites can greatly affect the dielectric properties [8–10]. Acceptor dopants are defined as ions with lower valency than the ions they replace, so Al ions can act as acceptor dopants (Al^{3+} on Ti^{4+} sites). Curve fitting have been used to fit the DC field dependence of the real part of the relative dielectric constant [11]. A. Outzourhit and J. U. Trefny [11] have investigated that the deviation from the behavior predicated by the theory of Devonshire [12] may be attributed to nonuniform dielectric constants throughout the samples which is tandem with the scanning electron microstructures.

In this paper, we have synthesized Al_2O_3-doped $(Ba_{0.6}Sr_{0.4})TiO_3$ powders using the conventional solid-state reaction. The $(Ba_{0.6}Sr_{0.4})TiO_3$ doped with different amount of Al_2O_3 have been found to be different from those of undoped $(Ba_{0.6}Sr_{0.4})TiO_3$. Curve fitting is used to fit the DC field dependence of the real part of the relative dielectric constant and the loss factor of all specimens. As the fitting is finished, the data obtained by measuring and curve fitting are compared and they may reveal more physical insights.

2. Experimental procedure

The starting raw chemicals were high-purity $BaCO_3$, TiO_2, $SrCO_3$ and Al_2O_3 powders. The composition prepared was $(Ba_{1-x}Sr_x)TiO_3$ with $x = 0.4$, hereafter referred to as BSTO. BSTO was doped with 0.5 wt%, 1.0 wt%, 1.5 wt%, 2.0 wt%, 5.0 wt%, 10 wt%, 15 wt% and 20 wt% Al_2O_3, these being referred to as shown in Table I. Specimens were prepared using the conventional mixed-oxide method. The raw material was weighed out in stoichiometric proportions, ball-milled in alcohol, dried and then calcined at 1150 °C for 3 h. The obtained powders were then crushed into a fine powder of less than 325 mesh and axially pressed into pellets having a diameter of 9.8 mm and thickness of 1.6 mm, prior to sintering at 1450 °C for 3 h. After sintering, the scanning electron microstructures (SEM) was employed to examine the microstructures of the specimens. Then the average grain size was determined from the microstructures of the specimens, as shown in Table I. The dielectric properties of the ceramic body were measured using a HP4194 impedance/gain phase analyzer. With the capacitance of the sample measured, the real part of the relative dielectric constant can be ε_r' calculated as

$$\varepsilon_r' = \frac{Cd}{A\varepsilon_0}, \tag{1}$$

where C is the capacitance, d is the thickness, A is the area and $\varepsilon_0 = 8.8542 \times 10^{-12}$ F/m. The % tunability is determined using the following equation

$$\%\,\text{tunability} = \frac{\varepsilon_r'(0) - \varepsilon_r'(V_{\text{app}})}{\varepsilon_r'(0)}, \tag{2}$$

where $\varepsilon_r'(0)$ is the real part of the relative dielectric constant without DC bias and $\varepsilon_r'(V_{\text{app}})$ is the real part of the relative dielectric constant bias with V_{app}. The tunability measurements were considered with the applied electric field which ranged from 0 to 1.5 KV/cm for all specimens.

Curve fitting is used to fit the DC field dependence of the real part of the relative dielectric constant and the loss factor of all specimens with Equations 3 and 5. The curve fittings employed are based on the least square method. In this method, the square of the deviation from the theoretical expectation to the experimental trend was calculated while varying the phenomenological coefficient. The fitting process is ended as the deviation is minimized at the specific value of the phenomenological coefficient.

TABLE I Sintered densities and grain sizes for all specimens (⋆ data unavailable for these specimens)

Sample	Al_2O_3 Content (wt%)	Density (g/cm^3)	Grain size (μm)
BSTO	0	5.589	3.94
BSTO1	0.5	5.383	10.58
BSTO2	1.0	5.210	25.71
BSTO3	1.5	5.147	19.93
BSTO4	2.0	5.059	11.23
BSTO5	5.0	4.993	8.95
BSTO6	10.0	4.506	7.2
BSTO7	15.0	4.410	⋆
BSTO8	20.0	3.892	⋆

3. Results and discussion

The sintered densities and grain size of all the specimens investigated are shown in Table I. The density and the grain size of the specimens were plotted as function of the Al_2O_3 doping contents as shown in Fig. 1. The density of the specimen decreases with increasing Al_2O_3 content, the grain size of specimens increases with Al_2O_3 content ≤ 1 wt% and decreases with Al_2O_3 content > 1 wt%.

The field dependence of the real part of the dielectric constant for all specimens were shown in the upper part of Fig. 2. The symbols for the data obtained by measuring and the lines for the data obtained by curve fitting. From the results of Fig. 2, the real part of the relative dielectric constant of the samples decreases with increasing the DC field. The tunability of the samples at 10 MHz, 20 MHz, 30 MHz, 40 MHz are listed in Table II. The tunability is defined as the changing percentage of the real part of the relative dielectric constant at 1.5 KV/cm. Variation of tunability with Al_2O_3 contents measuring at different frequencies is illustrated in Fig. 3. The tunability of the specimen increases with increasing Al_2O_3 contents for Al_2O_3 contents lower than 1 wt% and then decreases with increasing Al_2O_3 contents above 1 wt%. This is due to the fact that Devonshire's [10] theory assumes a stress free condition. However there is internal stress among grains

TABLE II The tunability at 10 MHz, 20 MHz, 30 MHz, 40 MHz for all specimens

Composition	10 MHz	20 MHz	30 MHz	40 MHz
BSTO1	10.11%	12.80%	12.91%	13.10%
BSTO2	10.83%	12.87%	17.04%	24.02%
BSTO3	10.09%	10.97%	11.27%	11.92%
BSTO4	8.35%	8.47%	8.11%	8.00%
BSTO5	3.91%	5.87%	7.89%	11.34%
BSTO6	3.96%	6.01%	5.91%	7.02%
BSTO7	2.94%	3.72%	2.59%	2.63%
BSTO8	2.60%	2.70%	2.80%	2.66%

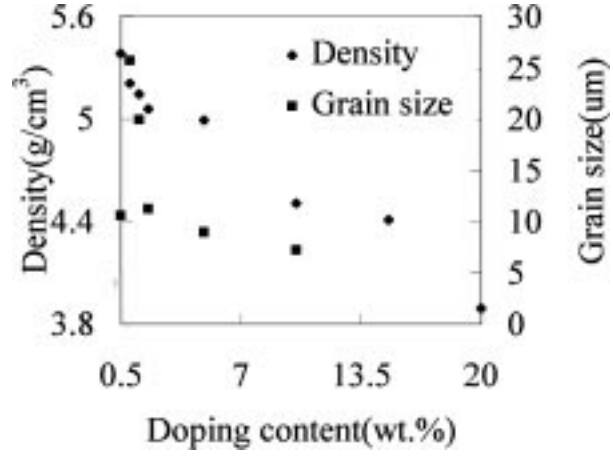

Figure 1 Density and grain size of the specimens as a function of Al_2O_3 doping content.

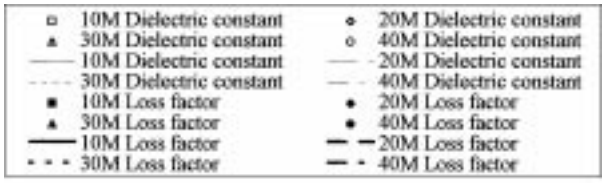

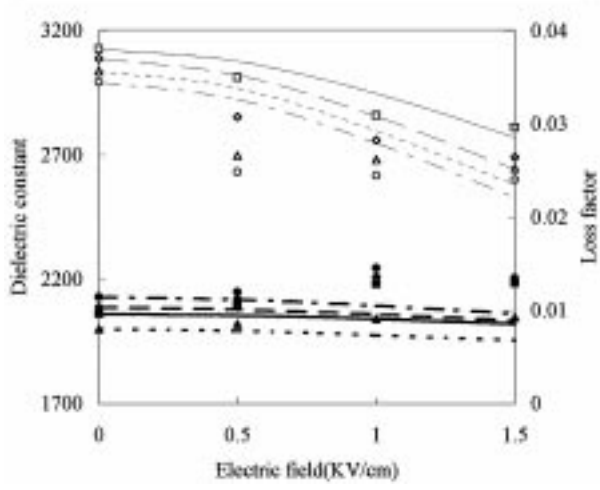

(a)

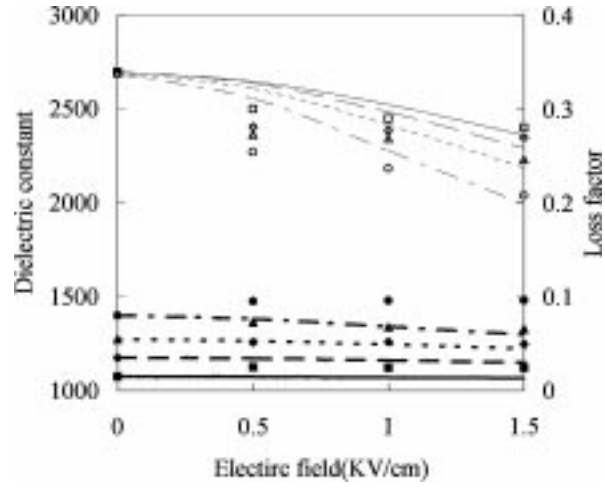

(b)

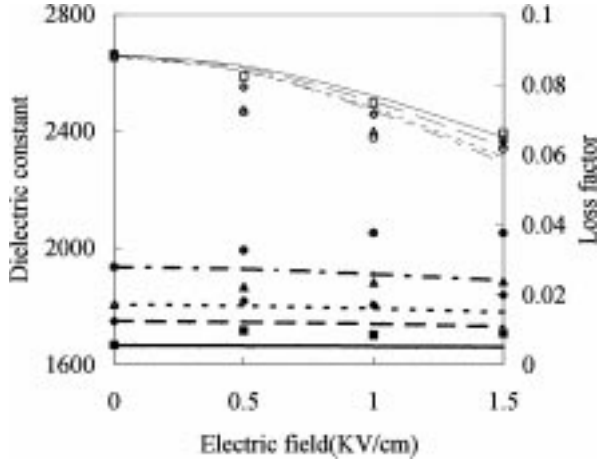

(c)

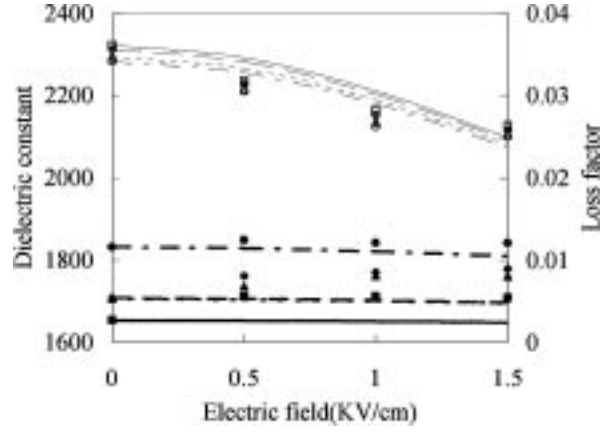

(d)

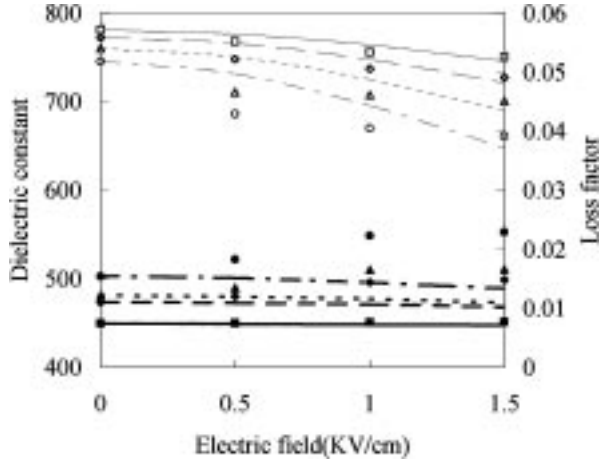

(e)

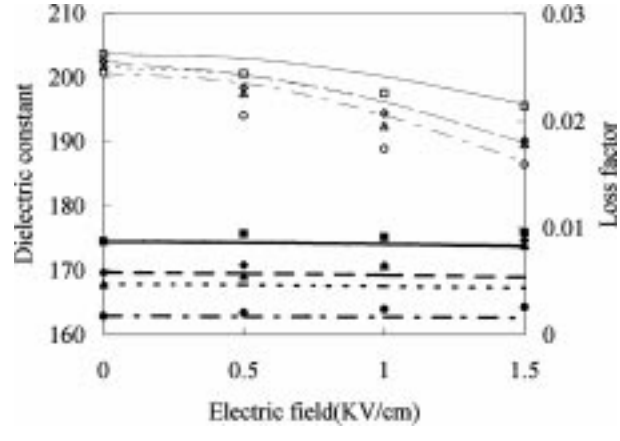

(f)

Figure 2 Dielectric constant and loss factor of all the specimens vs DC field at 10 MHz, 20 MHz, 30 MHz, 40 MHz. (a) BSTO1; (b) BSTO2; (c) BSTO3; (d) BSTO4; (e) BSTO5; (f) BSTO6; (g) BSTO7; (h) BSTO8. *(Continued)*.

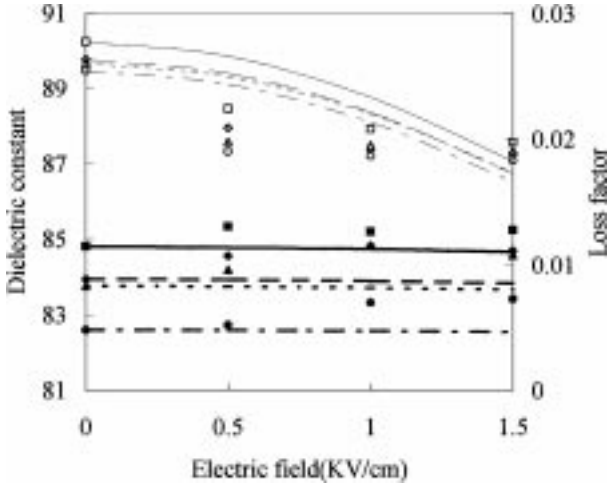

(g)

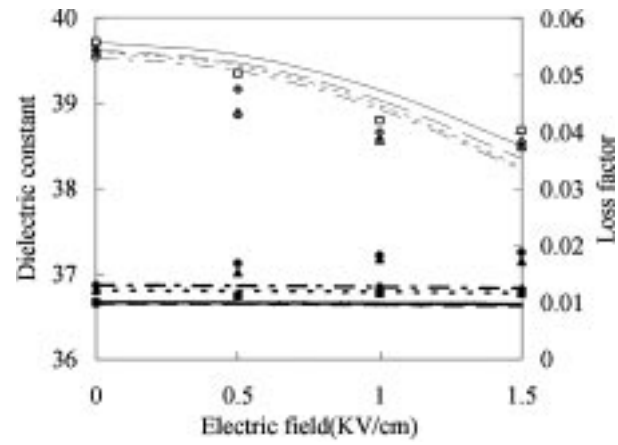

(h)

Figure 2 (Continued).

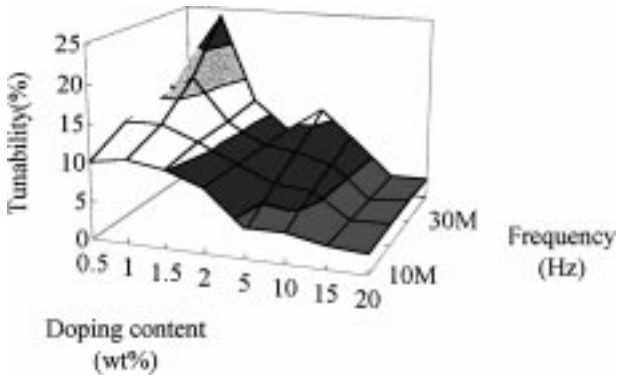

Figure 3 Variation of tunability (defined at 1.5 KV/cm) with Al_2O_3 content measuring at different frequencies.

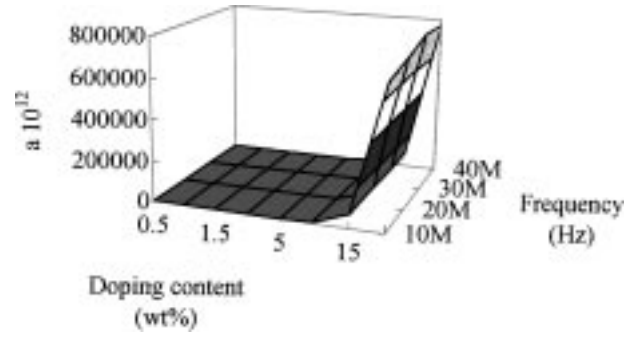

Figure 4 Variation of fitted phenomenological coefficients with Al_2O_3 content measuring at different frequencies.

affects the dielectric properties. The internal stress decreases with the increase of grain size. As a result of the grain size of BSTO2 is largest and the internal stress effect on BSTO2 should be smallest, the BSTO2 has maximum tunability. The samples with larger grains have larger tunability.

The real part of the relative dielectric constant ε_r' in paraelectric states was represented as [12]

$$\frac{\varepsilon_r'}{\varepsilon_{r0}'} = \frac{1}{\left(1 + a\varepsilon_{r0}'^3 E^2\right)^{1/3}}, \tag{3}$$

where ε_{r0}' and ε_r' are the real part of the relative dielectric constant under zero bias field and under bias field E; respectively; a is the phenomenological coefficient. The ε_r' of the samples decreases with increasing the bias field. The phenomenological coefficients obtained by curve fitting with Equation 3 are summarized in Table III. Variation of fitted phenomenological coefficients with Al_2O_3 doping contents at different frequencies is illustrated in Fig. 4. At Al_2O_3 doping contents below 10 wt%, the variation of fitted phenomenological coefficients with Al_2O_3 contents are small. At Al_2O_3 contents above 10 wt%, a rapid increase of the fitted phenomenological coefficient occurs. The value of fitted phenomenological coefficient is influenced by the real part of the relative dielectric constant under zero bias field. At high Al_2O_3 contents, such as above 10 wt.%, where the suppression of ε_{r0}' is remarkable. Therefore, the fitted phenomenological coefficient of samples with smaller ε_{r0}' is larger to keep a $\varepsilon_{r0}'^3$ being a reasonable value.

As shown in the bias equation (Equation 3), the phenomenological coefficient of the DC field E is the product of a $\varepsilon_{r0}'^3$. The phenomenological coefficient are used to determine the effects of the DC field on the real part of the relative dielectric constant. It is convenient to define a field coefficient A which represents the strength of the DC field effect. Thus the bias equation for the real part of the relative dielectric constant is re-written as:

$$\frac{\varepsilon_r'}{\varepsilon_{r0}'} = \frac{1}{(1 + AE^2)^{1/3}} \tag{4}$$

TABLE III The phenomenological coefficient $\times 10^{12}$ at 10 MHz, 20 MHz, 30 MHz, 40 MHz for all specimens

Composition	10 MHz	20 MHz	30 MHz	40 MHz
BSTO1	6.33	8.94	10.00	10.89
BSTO2	11.00	14.10	19.47	32.83
BSTO3	9.36	10.73	12.10	13.08
BSTO4	12.56	12.58	12.40	12.42
BSTO5	138.57	220.69	344.67	562.05
BSTO6	7656.90	11850.92	12268.65	15486.36
BSTO7	68039.06	66210.57	62975.62	64926.30
BSTO8	689427.86	731147.39	780713.49	769777.41

The field coefficients A are summarized in Table IV. As shown in Fig. 5, variation of A with Al_2O_3 contents has the same trend as that of grain size as shown in Fig. 1.

The real part of the relative dielectric constant obtained by curve fitting with the bias equation as shown in the upper part of Fig. 2. The fitting of the measured dielectric constants by Equation 3 is poor for all the specimens. For the specimens, the real part of the relative dielectric constant by measuring is larger than the data obtained by curve fitting at 1.5 KV/cm and smaller than the data obtained by curve fitting at 0.5 KV/cm and 1.0 KV/cm. The difference between the data obtained by measuring and curve fitting at 0.5 KV/cm is larger than at 1.0 KV/cm.. Compare to the data obtained by curve fitting, the real part of the relative dielectric constant decreases rapidly with the applied electric field up to fields at 0.5 KV/cm or 1 KV/cm. The real part of the relative dielectric constant decreases slowly after 1 KV/cm are observed in the plot.

This is due to the fact that the specimens of Al_2O_3-doped BSTO are semi-conductive and the measured dielectric properties are caused by the space charge polarization. In the Heywang model [13–16], oxygen ions are adsorbed on the grain boundaries in a concentration N_S (m^{-2}) as shown in Fig. 6. These attracting electrons from the surface layers of the crystallites. A surface charge of $-2QN_S$ (m^{-2}) is formed, along with two space -charge layers with a thickness $b = N_S/n_i$ where n_i is the bulk electron concentration. The electrical potential Ψ_x varies in these depletion layers as:

$$\frac{q\Psi_x}{KT} = -\frac{n_1 q^2}{2\varepsilon_0 \varepsilon_r KT}(b-x)^2, \tag{5}$$

TABLE IV The field coefficient A at 10 MHz, 20 MHz, 30 MHz, 40 MHz for all specimens

Composition	10 MHz	20 MHz	30 MHz	40 MHz
BSTO1	0.1933	0.2631	0.2802	0.2920
BSTO2	0.2157	0.2769	0.3796	0.6378
BSTO3	0.1763	0.2019	0.2261	0.2454
BSTO4	0.1571	0.1553	0.1495	0.1477
BSTO5	0.0660	0.1018	0.1515	0.2330
BSTO6	0.0647	0.0984	0.1006	0.1252
BSTO7	0.0500	0.0479	0.0454	0.0465
BSTO8	0.0432	0.0455	0.0485	0.0476

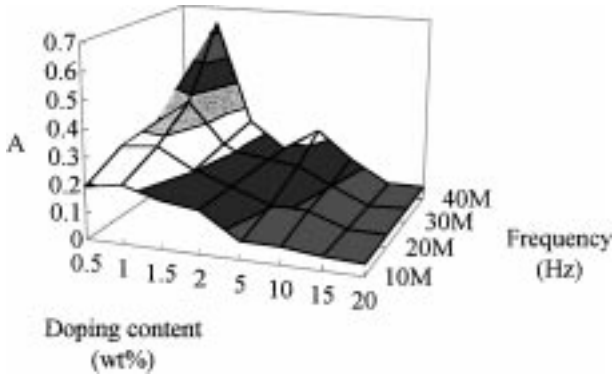

Figure 5 Variation of field coefficient A with Al_2O_3 content measuring at different frequencies.

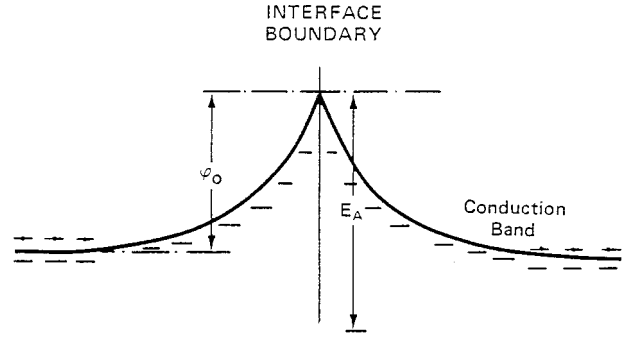

Figure 6 Heywang grain-boundary barrier model [11–14].

where q represents the positive elementary charge, ε_r is the relative dielectric constant and x is the distance to the boundary.

Park and Payne [17] proposed an equivalent $n-c-i-c-n$ microstructures at each grain boundaries in extending the Heywang barrier modal. A proposed energy band model grain boundary layer (GBL) capacitors is given in Fig. 7. The diagram is for unbiased thermal equilibrium. It represents the $n-c-i-c-n$ model for IBL phenomena with the possible formation of compensation (c) layers between n-type grains and insulating (i) grain boundaries. The potential barrier (V_B) for the junction in this modal is similar to a Schottky modal. C_C^F and C_C^R for forward and reverse bias capacitance per unit area on either side of an insulating barrier of width 2δ. On application of a bias voltage, the barrier is lowered ($V_B - V$) in the forward sense and raised ($V_B + V$) in the reverse case. The total series capacitance (C_S) per unit area is given by the capacitance of the insulating layer (C_i) and the series connected forward (C_C^F) and reverse (C_C^R) biased compensation layers:

$$\frac{1}{C} = \frac{1}{C_i} + \frac{1}{C_C^F} + \frac{1}{C_C^R}, \tag{6}$$

which is expanded as

$$\frac{1}{C} = \frac{2\delta}{\varepsilon_0 K_i} + \left[\frac{2(V_B - V)}{qN_D + \varepsilon_0 K_C}\right]^{1/2} + \left[\frac{2(V_B + V)}{qN_D + \varepsilon_0 K_C}\right]^{1/2}, \tag{7}$$

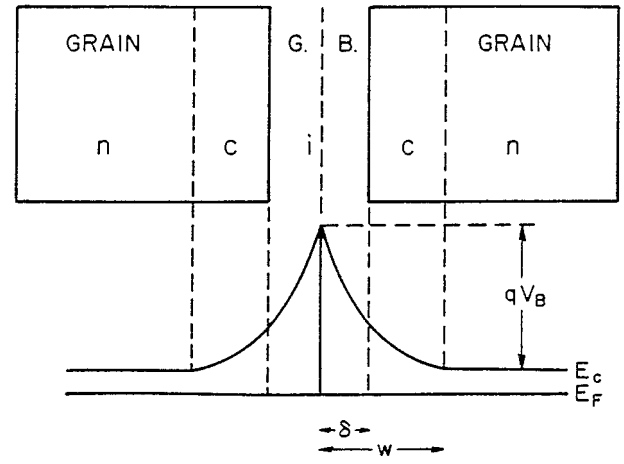

Figure 7 Energy band diagram for an equivalent $n-c-i-c-n$ grain-boundary barrier model [15].

where ε_0 is the permittivity of the free space, K_i and K_C are the relative dielectric constant of the insulating and compensation layers, q is the electronic charge and N_D is the concentration of uncompensated ionized donors. At $V = 0$, for a symmetric barrier,

$$\frac{1}{C} = \frac{2\delta}{\varepsilon_0 K_i} + 2\left[\frac{2V_B}{qN_D + \varepsilon_0 K_C}\right]^{1/2}, \quad (8)$$

Below the break point, $V < V_B$, the C-V curve will be effected by the forward bias capacitance and reverse bias capacitance. Above the CV break point, $V > V_B$, the forward biased junction is saturated and reverse biased capacitance dominates.

$$\frac{1}{C} = \frac{2\delta}{\varepsilon_0 K_i} + \left[\frac{2(V_B + V)}{qN_D + \varepsilon_0 K_C}\right]^{1/2}, \quad (9)$$

Due to the theory depicted above, the real part of the relative dielectric constant decreases rapidly below the break point and decreases slowly above the break point. The break point of BSTO1 to BSTO8 is between 0.5 KV/cm and 1.0 KV/cm.

The loss factor obtained by measuring and curve fitting with the bias equation as shown in the lower part of Fig. 2. The symbols and the lines for the loss factor obtained by measuring and curve fitting. The loss factor obtained by measuring is larger than the data obtained by curve fitting. The difference between the data obtained by measuring and curve fitting increases with increasing applied electric field. The intrinsic dielectric loss $\tan\delta_C$ can be expressed as [12]:

$$\frac{\tan\delta_c}{\tan\delta_{co}} = \frac{1}{\left[1 + a\varepsilon_{r0}'^3 E^2\right]^{1/3}}, \quad (10)$$

where $\tan\delta_{CO}$ and $\tan\delta_C$ are the loss factor under zero bias field and under bias field E, a is the phenomenological coefficient. The $\tan\delta_C$ of the samples decreases with increasing the bias field. However, the loss factor of the specimen by measuring under bias DC field is larger then that under zero bias field. It is inferred that there must be another loss mechanism increasing with increasing the bias field for the dielectric loss. This can be explained by the capacitor circuit model. With the capacitor circuit model, there is a conduction loss mechanism other than the intrinsic dielectric loss. The loss factor $\tan\delta$ is expressed as:

$$\tan\delta = \tan\delta_C + \tan\delta_R, \quad (11)$$

$$\tan\delta_R = \frac{1}{\omega RC}, \quad (12)$$

The $\tan\delta_R$ is the conduction loss increasing with increasing the DC field.

4. Conclusions

Composites of BSTO and Al_2O_3 ceramics have been fabricated and characterized. The composites have adjustable dielectric properties. It is inferred that the tunability of the specimen is affected by the grain size. The real part of the relative dielectric constant of the samples decreases with increasing the bias electric field. Phenomenological coefficients is independent with Al_2O_3 contents below 10 wt.% and a rapid increase occurs above 10 wt.%. Variation of field coefficient A and tunability with Al_2O_3 contents has the same trend as that of the grain size. The curve fitting is only well for BSTO and poor for others. This is due to the fact that the specimens of Al_2O_3-doped BSTO are semi-conductive and the difference between measuring and curve fitting can be explained by the space charge polarization theory. There is a conduction loss mechanism other than the intrinsic dielectric loss for the dielectric loss under bias electric field.

Acknowledgments

This work was supported by the National Science Council of Republic of China under contact NSC-87-2218-E-006-060.

References

1. F. D. FLAVIIS, N. G. ALEXOPOULOS and O. M. STAFSUDD, *IEEE Transactions on Microwave Theory and Techniques* **45**(6) (1997) 963.
2. S. STOWELL, L. C. SENGUPTA, E. NGO, M. E. O'DAY and R. LANCO, in ISAF'94. Proceedings of the Ninth IEEE International Symposium on Applications of Ferroelectric, 1994, p. 372.
3. L. C. SENGUPTA, E. NGO, M. E. O'DAY, S. STOWELL and R. LANCO, in ISAF'94. Proceedings of the Ninth IEEE International Symposium on Applications of Ferroelectric, 1994, p. 622.
4. L. WU, Y. C. CHEN, Y. P. CHOU, Y. T. TSAI and S. Y. CHU, in *J. J. Appl. Phys.*, accepted for publication.
5. X. H. WANG, Z. L. GUI and L. T. LI, *Materials Chemistry and Physics* **55** (1998) 193.
6. S. B. HERNER, F. A. SELMI, V. V. VARADAN and V. K. VARADAN, *Materials Letters* **15** (1993) 317.
7. L. WU, Y. C. CHEN, Y. P. CHOU, Y. T. TSAI and S. Y. CHU, in *J. J. Appl. Phys.* **38** (1999), accepted for publication.
8. H. M. CHAN, M. P. HARMER and D. M. SMYTH, *J. Amer. Ceram. Soc.* **69** (1986) 507.
9. S. B. DESU and D. A. PAYEN, *ibid.* **73**(11) (1990) 3391.
10. Y. M. CHIANG and T. TAKAGI, *ibid.* **73**(11) (1990) 3278.
11. A. OUTZOURHIT and J. U. TREFNY, *J. Mater. Res.* **10**(6) (1995) 1411.
12. K. M. JOHNSON, *J. Appl. Phys.* **33** (1961) 2826.
13. W. HEYWANG, *Solid State Phys.* **4** (1960) 877.
14. *Idem., Solid State Electr.* **3**(1) (1961) 51.
15. *Idem., J. Amer. Ceram. Soc.* **47**(10) (1964) 484.
16. *Idem., J. Mater. Sci.* **6** (1971) 1214.
17. H. D. PARK and D. A. PAYNE, in "Grain Boundary Phenomena in Electronic Ceramics Vol. 1," American Ceramic Society, Columbus, OH, 1981) p. 242.

Received 12 August 1999
and accepted 24 April 2000